Scripta Materialia 116 (2016) 147–151

Contents lists available at ScienceDirect

Scripta Materialia

journal homepage: www.elsevier.com/locate/scriptamat

Regular Article

Effects of crystallographic orientation on the superelastic response of FeMnAlNi single crystals

L.W. Tseng [a], Ji Ma [b], S.J. Wang [b], I. Karaman [a,b,*], Y.I. Chumlyakov [c]

[a] Department of Mechanical Engineering, Texas A&M University, College Station, TX 77843, USA
[b] Department of Materials Science and Engineering, Texas A&M University, College Station, TX 77843, USA
[c] Tomsk State University, Siberian Physical Technical Institute, Tomsk 634050, Russia

ARTICLE INFO

Article history:
Received 1 November 2015
Received in revised form 18 January 2016
Accepted 23 January 2016
Available online 19 February 2016

Keywords:
FeMnAlNi
Superelasticity
Single crystals
Martensite variants
Iron-based shape memory alloys

ABSTRACT

The effects of crystal orientation on the tensile superelastic response of the $Fe_{43.5}Mn_{34}Al_{15}Ni_{7.5}$ single crystalline shape memory alloy, oriented along the <100> and <123> directions were investigated. The single crystals aged at 200 °C for 3 h demonstrated superelastic strains of 3.6% along the <100> orientation and 7.8% along the <123> orientation. Although the theoretical transformation strain in the <100> orientation is higher than that in the <123> orientation, the <123> oriented single crystals demonstrate better superelastic recovery in tension due to a higher number of active martensite variants, which promote better accommodation of internal strains and help minimize defect formation during transformation.

NiTi based shape memory alloys (SMAs) are widely used in industrial and medical applications. However, NiTi is expensive and difficult to cold work, therefore many attempts have been made to produce iron-based SMAs such as Fe–Ni and Fe–Mn based ones with lower material cost and better cold workability. However, superelastic recovery in FeMnSi, FeNiCoTi and FeMnAl SMAs [1–3] was historically poor. Recently, Tanaka et al. [4] and Omori et al. [5] discovered novel nano-precipitation hardened $Fe_{40.95}Ni_{28}Co_{17}Al_{11.5}Ta_{2.5}B_{0.05}$ (at.%) and $Fe_{43.5}Mn_{34}Al_{15}Ni_{7.5}$ (at.%) SMAs, respectively, with impressive superelastic recovery levels. The former showed 13.5% superelastic strain at room temperature through an fcc (austenite) to bct (martensite) martensitic transformation. The latter showed 5% superelastic strain through a bcc (austenite) to an fcc (martensite) martensitic transformation. Following these studies, several additional iron-based SMAs such as single crystal forms of $Fe_{41}Ni_{28}Co_{17}Al_{11.5}Ta_{2.5}$ [6–9], $Fe_{41}Ni_{28}Co_{17}Al_{11.5}Nb_{2.5}$ [10], $Fe_{41}Ni_{28}Co_{17}Al_{11.5}Ti_{2.5}$ [11], $Fe_{43.5}Mn_{34}Al_{15}Ni_{7.5}$ [12,13], and polycrystalline $Fe_{40.95}Ni_{28}Co_{17}Al_{11.5}Ti_{2.5}B_{0.05}$ [14], $Fe_{40.95}Ni_{28}Co_{17}Al_{11.5}Nb_{2.5}B_{0.05}$ [15], and $Fe_{43.5}Mn_{34}Al_{15}Ni_{7.5}$ [16] were also reported to show 4–6% recoverable strain. Of particular interest is the $Fe_{43.5}Mn_{34}Al_{15}Ni_{7.5}$ alloy, which shows a small temperature dependence of the superelastic stress for stress-induced martensitic transformation in a wide temperature range from −196 to 240 °C [5]. In this material, highly reversible superelasticity is facilitated by the formation of precipitates around 10 nm that are coherent with both the austenite and martensite phases [17].

Crystal orientation, and thus crystallographic texture, is known to be one of the important factors that influence the superelastic response of the SMAs. Studies on NiTi single crystals by Gall et al. [18,19] showed that the superelastic response of NiTi SMAs is strongly dependent on the crystallographic orientation: under tension, the <100> orientation demonstrates smaller transformation strain and higher critical stress than those in the <111> orientation, and an opposite response is observed under compression [18,19]. In FeNiCoTi SMAs, Sehitoglu et al. [2] reported that the <123> oriented single crystal exhibits higher recoverable strain than that in the <100> orientation under both tension and compression. In our previous study, $Fe_{43.5}Mn_{34}Al_{15}Ni_{7.5}$ (at.%) single crystals oriented along the <100> direction showed poor superelastic recovery in tension due to the large volume fraction of retained martensite pinned by dislocations both within the austenite matrix and at the austenite–martensite interfaces [12]. On the other hand, much better recovery was observed under compression. We demonstrated that the discrepancy was caused by a difference in martensite variant selection under tension and compression. Whereas only one martensite variant can accommodate tensile deformation along the <100> direction, two martensite variants can accommodate deformation in compression [12]. Since the martensite variants available for the accommodation of strain depend strongly on the direction of loading, it is important to characterize the FeMnAlNi single crystals in different crystallographic orientations to understand the orientation dependence of the superelastic response. This understanding will be

* Corresponding author at: Department of Materials Science and Engineering, Texas A&M University, College Station, TX 77843, USA.
E-mail address: ikaraman@tamu.edu (I. Karaman).

http://dx.doi.org/10.1016/j.scriptamat.2016.01.032
1359-6462/

beneficial for the prediction of the superelastic behavior in textured polycrystals. In this work, we study the $Fe_{43.5}Mn_{34}Al_{15}Ni_{7.5}$ (at.%) single crystals aged at 200 °C for 3 h along the <100> and <123> orientations to investigate the orientation dependence of superelastic response. The particular aging heat treatment was selected to obtain less than 10 nm nano-precipitates in the microstructure.

Single crystal samples with a nominal composition of $Fe_{43.5}Mn_{34}Al_{15}Ni_{7.5}$ (at.%) were grown using the Bridgman technique in a helium atmosphere. Flat dog-bone-shaped tensile samples with the gauge dimensions of 1.5 mm × 3 mm × 8 mm were cut using wire electro-discharge machining (EDM) from the single crystals with the tension axis parallel to the <100> or <123> orientations. The tension samples were sealed into quartz tubes under high purity argon atmosphere and solution heat treated at 1200 °C for 1 h followed by water quenching. Subsequently, the crystals were aged at 200 °C for 3 h under ultra-high purity argon atmosphere to introduce coherent B2 (bcc/NiAl) precipitates into the austenite matrix. Transmission electron microscopy (TEM) samples were prepared by twin-jet electro-polishing with a solution of 30% volume nitric acid and 70% volume methanol mixture at −20 °C. TEM investigations were conducted using a FEI Tecnai G^2 F20 electron microscope.

The superelastic response of the aged crystals was characterized via the incremental tensile testing at room temperature. Before performing the mechanical testing, the samples were mechanically polished. In this test, 2% tensile strain is first applied on the sample followed by complete unloading. Thereafter, the applied strain level was increased during each subsequent loading–unloading cycle until the sample fractured. These experiments were performed with a servo-hydraulic MTS test frame at a strain rate of $5 \times 10^{-4}\ s^{-1}$. An extensometer was directly attached to the gauge section of the samples to measure the axial strain.

The calculated transformation strains as function of crystal orientation in tension are displayed in Fig. 1. The transformation strains were calculated using energy minimization theory (for CVP strains, Fig. 1a) [20] and lattice deformation theory (for detwinning strains, Fig. 1b) [21]. The energy minimization approach assumes that the single crystal austenite transforms into martensite forming twinned martensite [20], while the lattice deformation approach assumes that the single crystal austenite transforms to single crystal martensite without internal twinning [21]. More detailed description of these theoretical frameworks can be found in [22–26]. Taking lattice parameters of austenite and martensite as 0.2903 nm and 0.3672 nm, respectively from [5], the calculated transformation strains with detwinning are found to be 26.5% and 14%, and the calculated CVP strains are 10.5% and 9% for the <100> and <123> orientations, respectively.

Fig. 2a and b show the tensile stress–strain responses of the $Fe_{43.5}Mn_{34}Al_{15}Ni_{7.5}$ single crystals with the <100> and <123> orientations. The sample with the <100> orientation shows partial recovery until a stress drop at about 6% applied strain, after which recovery is no longer observed. The result suggests a large amount of retained martensite [12]. On the other hand, the sample with the <123> orientation is almost fully reversible up to 8% applied strain. The sample was fractured at 9% applied strain. The relationship between the recoverable and applied strains in both <100> and <123> orientations is summarized in Fig. 2c. From these results, the recoverable strain in the <123> orientation is nearly perfect up to 8% of applied strain and the maximum recoverable strain is approximately 7.8%, comparable to the calculated 9% expected for the CVP strain. However, the maximum recoverable strain in the <100> orientation is only 3.5%. The experimental value is far smaller than the theoretical transformation strain in this orientation, which is 10.5% for CVP and 26.5% for the fully detwinned condition.

Although the <100> orientation has higher theoretical transformation strain than that in the <123> orientation under tension, the <123> orientation shows higher recoverable strain than the former. In order to study the reason behind this difference, TEM investigation is carried out on the tensile samples with the <100> and <123> orientations after the tensile tests at room temperature. Because the tension

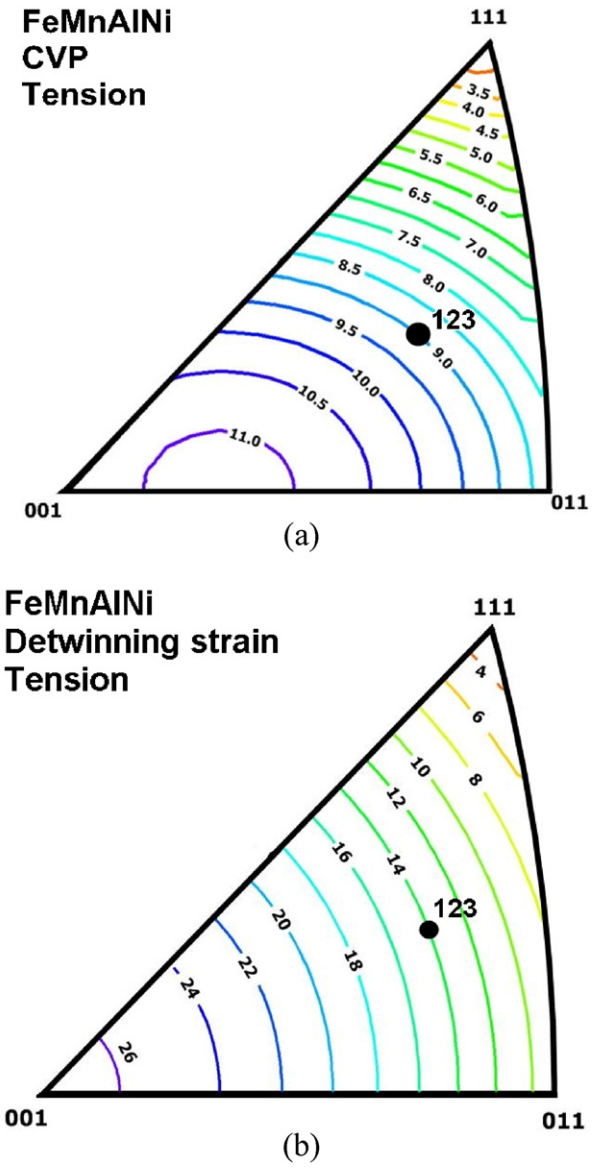

Fig. 1. Calculated orientation dependence of the transformation strains in tension for the $Fe_{43.5}Mn_{34}Al_{15}Ni_{7.5}$ single crystals assuming: (a) internally twinned martensite and (b) fully detwinned martensite. See text for details on the calculations.

sample with the <100> orientation after the completion of incremental strain test is almost fully martensitic, it is difficult to locate the austenite–martensite boundary. Therefore, we performed an experiment where a tensile sample was loaded to 8% instead, such that the martensite–austenite boundary could be more easily captured (inset, Fig. 2a). Fig. 3 shows the bright field TEM image of the sample with the <100> orientation after the 8% strain (inset, Fig. 2a). From the TEM results, high density of parallel dislocations and hairpin-shaped dislocations are generated at the austenite–martensite interface and in the austenite matrix, respectively. This kind of deformation microstructures were previously reported in studies on FeMnAlNi single crystals with the <100> orientation [12] and on FeNiCoTi polycrystals [27].

Fig. 4a shows the bright field TEM image of the solution-treated single crystals with the <123> orientation after 4% strain at room temperature (inset, Fig. 2b). A solution-treated sample was tested because aged samples show excellent superelastic recovery, making it difficult to obtain an austenite–martensite two-phase structure that makes it possible to study both the martensite structure and the austenite–martensite interface. The selection of 4% applied strain is based on the superelastic

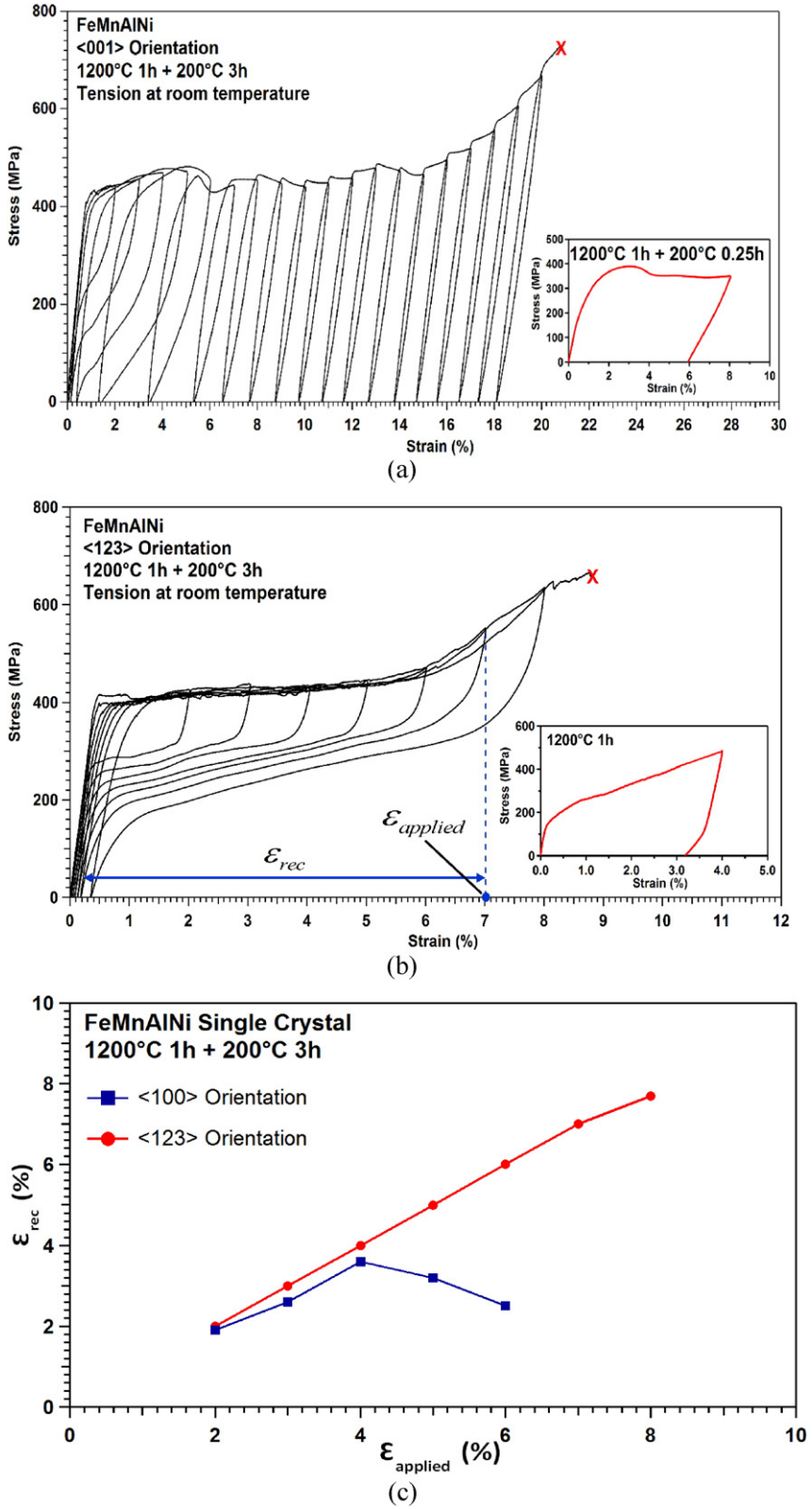

Fig. 2. Superelastic response of $Fe_{43.5}Mn_{34}Al_{15}Ni_{7.5}$ single crystals aged at 200 °C for 3 h under incremental tensile strain tests at room temperature along the (a) <100> and (b) <123> orientations. The insets in (a) and (b) shows the testing condition for the samples examined with TEM shown in Figs. 3 and 4; (c) recoverable strains as a function of applied strains along the <100> and <123> orientations. ε_{rec} and $\varepsilon_{applied}$ represent the total recoverable strain and applied tensile strain, respectively.

response of the aged sample, shown in Fig. 2b. The maximum superelastic strain of the aged sample is around 9%. Applying the 4% strain is nearly half of this value and ensures a similar martensite/austenite volume fraction compared to the <100> sample studied with TEM. Two martensite variants can be seen from the bright field TEM image. The corresponding selected-area electron diffraction (SAED) patterns of two martensite variants are shown in Fig. 4b. Fig. 4c shows the high magnification bright field TEM image at the austenite–martensite

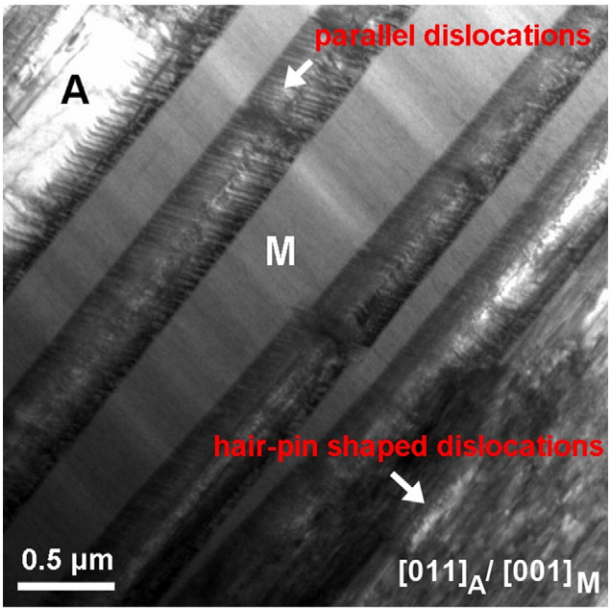

Fig. 3. Bright field TEM image of $Fe_{43.5}Mn_{34}Al_{15}Ni_{7.5}$ single crystals, aged at 200 °C for 0.25 h, oriented along the <100> direction after 8% tensile strain at room temperature.

interface. While few dislocation loops and bend contours are observed, the dislocation density is very low as compared to the samples with the <100> orientation. The austenite–martensite boundary appears sharp and clean, and parallel dislocations and hairpin-shaped dislocations shown in Fig. 3 were not observed in any zone axes.

The high density of parallel dislocations at the austenite–martensite interface and hairpin-shaped dislocations in the austenite matrix in the <100> single crystals, shown in Fig. 3, pin the martensite phase and cause poor superelastic recovery. The reason for the formation of such dislocations is likely related to internal stress generated during martensitic transformation and the number of martensite variants active during the stress-induced transformation: based on the crystallography of the transformation, only one martensite variant is available to accommodate tensile strain along the <100> orientation. This makes it difficult to accommodate lattice mismatch between the austenite and martensite, and thus results in the creation of dislocations that pin the martensite. On the other hand, two martensite variants are observed in the tension sample with the <123> orientation, making it possible for martensite to easily form twins to accommodate the lattice strains, and reducing the likelihood of dislocation formation. The similar observations were also reported in the FeMnAlNi compression samples with the <100> orientation [12] and in the FeNiCoAlTa and FeNiCoAlTi single crystals oriented along the <100> direction under tension [7,9,11].

The fracture strain for the tension sample oriented along the <123> direction is about 9% (Fig. 2b), at which point hardening in the stress–strain curve is also observed — suggesting the sample approaches the end of the transformation. This value is closer to the calculated CVP strain in the <123> orientation than the calculated detwinning value (Fig. 1), which suggests that the martensite adopts a twinned morphology in the <123> orientation during tensile deformation (Fig. 4a). In contrast to the <123> orientation, the fracture strain in the <100> is about 21% and is closer to the calculated detwinning strain while far exceeding the maximum CVP strain. The result suggests that the martensite morphology in the <100> orientation is single-variant morphology. These observations provide a potential explanation for the differences between the superelastic response of the <100> and <123> oriented single crystals in tension.

Finally, it is possible that the differences in superelastic reversibility could also be related to the inherent ability of the single crystals to resist plastic deformation in different orientations. Based on the Schmid Law,

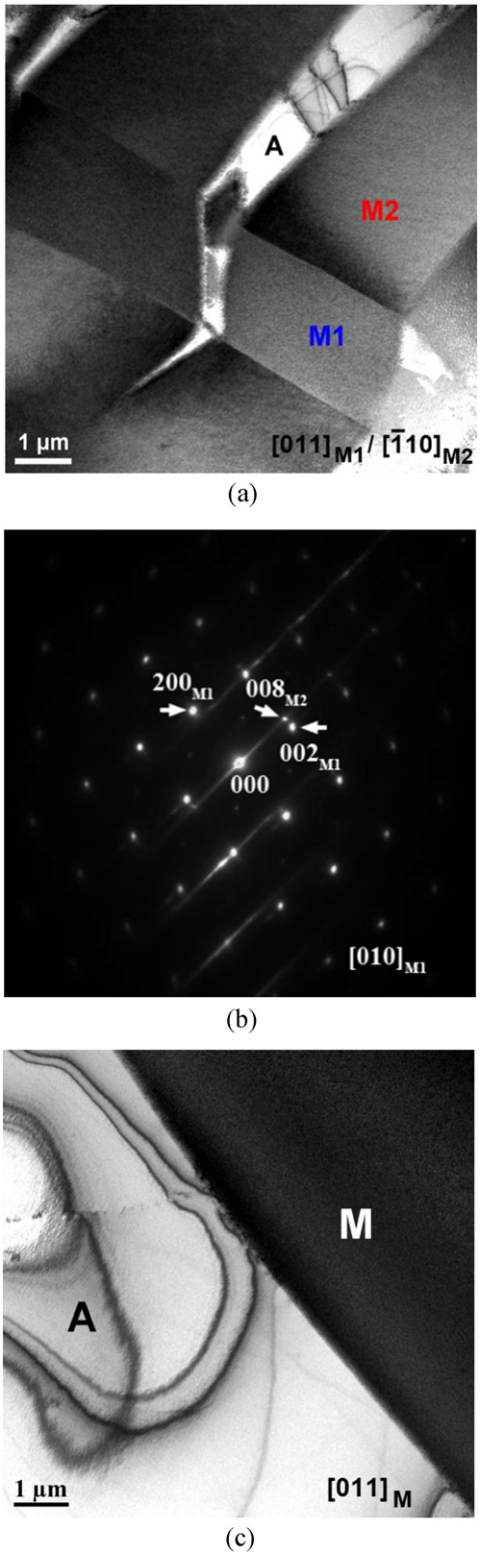

Fig. 4. TEM micrographs in the $Fe_{43.5}Mn_{34}Al_{15}Ni_{7.5}$ solution-treated single crystals oriented along the <123> direction after 4% tensile strain at room temperature: (a) the bright field TEM image showing two martensite variants. (b) The SAED patterns of martensite variants M1 and M2, shown in Fig. 4a. In this diffraction condition, the electron beam is parallel to [010] zone axis of M1 but it cannot be parallel to any low indexing zone axis of M2 at the same time. As a result, there is just one basic reciprocal vector, $(008)_{M2}$, that can be found in the diffraction pattern. (c) The austenite–martensite interface.

the Schmid factor for dislocation slip is similar in the <100> and <123> orientations through pencil glide [28]. However, it is also known that deformation in bcc metals often do not adhere to the Schmid law, which results, among other unusual characteristics, a stronger-than-expected orientation dependence of dislocation motion and tension–compression asymmetry, that are both sensitive to temperature [29–30]. It is currently not known how such phenomenon is manifested in the bcc FeMnNiAl austenite, but it is possible that dislocation activity may be easier in <100> orientation compared to <123> or vice versa despite similar Schmid factors. This contribution will be a subject of a future study.

In the present study, the superelastic response of $Fe_{43.5}Mn_{34}Al_{15}Ni_{7.5}$ <100> and <123> oriented single crystals was investigated under tension. The tensile samples aged at 200 °C for 3 h oriented in the <100> and <123> directions show 3.5% and 7.8% recoverable superelastic strains at room temperature, respectively. Poor recoverable strain in the <100> orientation is due to the formation of the high density of parallel dislocations in the austenite matrix and hairpin-shaped dislocations at the austenite–martensite interface due to an insufficient martensite variant activation. In the <123> orientation, the ability to easily form two martensite variants provides a mechanism to accommodate applied deformation and suppresses the need for massive dislocation formation. As a result, high mobility of austenite-martensite interfaces leads to high superelastic strains in the <123> orientation.

Acknowledgments

This work was supported by the U.S. National Science Foundation — International Materials Institute Program through the Grant No. DMR 08-44082. YIC acknowledges the support from The Tomsk State University D.I. Mendeleev Fund Program.

References

[1] A. Sato, E. Chishima, K. Soma, T. Mori, Acta Metall. 30 (1982) 1177.
[2] H. Sehitoglu, I. Karaman, X.Y. Zhang, Y. Chumlyakov, H.J. Maier, Scr. Mater. 44 (2001) 779.
[3] K. Ando, T. Omori, T. Ohnuma, R. Kainuma, Appl. Phys. Lett. 95 (2009) 212504.
[4] Y. Tanaka, Y. Himuro, R. Kainuma, Y. Sutou, K. Ishida, Science 327 (2010) 1488.
[5] T. Omori, K. Ando, M. Okano, X. Xu, Y. Tanaka, I. Ohnuma, R. Kainuma, K. Ishida, Science 333 (2011) 68.
[6] J. Ma, B. Kockar, A. Evirgen, I. Karaman, Z.P. Luo, H. Sehitoglu, C. Efstathiou, H.J. Maier, Y.I. Chumlyakov, Acta Mater. 60 (2012) 2186.
[7] J. Ma, B.C. Hornbuckle, I. Karaman, G.B. Thompson, Z.P. Luo, Y.I. Chumlyakov, Acta Mater. 61 (2013) 3445.
[8] A. Evirgen, J. Ma, I. Karaman, Z.P. Luo, Y.I. Chumlyakov, Scr. Mater. 67 (2012) 475.
[9] P. Krooß, C. Somsen, T. Niendorf, M. Schaper, I. Karaman, Y.I. Chumlyakov, G. Eggeler, H.J. Maier, Acta Mater. 79 (2014) 126.
[10] Y.I. Chumlyakov, I.V. Kireeva, O.A. Kuts, D.A. Kuksgauzen, Russ. Phys. J. 57 (2015) 1328.
[11] L.W. Tseng, Ji Ma, I. Karaman, S.J. Wang, Y.I. Chumlyakov, Scr. Mater. 101 (2015) 1.
[12] L.W. Tseng, Ji. Ma, S.J. Wang, I. Karaman, M. Kaya, Z.P. Luo, Y.I. Chumlyakov, Acta Mater. 89 (2015) 37.
[13] L.W. Tseng, Ji. Ma, B.C. Hornbuckle, I. Karaman, G.B. Thompson, Z.P. Luo, Y.I. Chumlyakov, Acta Mater. 97 (2015) 234.
[14] D. Lee, T. Omori, R. Kainuma, Alloys Compd. 617 (2014) 120.
[15] T. Omori, S. Abe, Y. Tanaka, D.Y. Lee, K. Ishida, R. Kainuma, Scr. Metall. 69 (2013) 812.
[16] M. Vollmer, C. Segel, P. Krooß, L.W. Tseng, J. Günther, I. Karaman, A. Weidner, H. Biermann, T. Niendorf, Scr. Mater. 108 (2015) 23.
[17] T. Omori, M. Nagasako, M. Okano, K. Endo, R. Kainuma, Appl. Phys. Lett. 101 (2012) 231907.
[18] K. Gall, H. Sehitoglu, Y.I. Chumlyakov, I.V. Kireeva, H.J. Maier, J. Eng. Mater. Technol. 1999A (1999) 121.
[19] K. Gall, H. Sehitoglu, Y.I. Chumlyakov, I.V. Kireeva, Acta Mater. 47 (1999) 1203.
[20] J.M. Ball, R.D. James, Arch. Ration. Mech. Anal. 100 (1987) 13.
[21] T. Saburi, S. Nenno, Pittsburgh, 100 1981, p. 1455.
[22] R.D. James, K.F. Hane, Acta Mater. 48 (2000) 197.
[23] J.M. Ball, Mater. Sci. Eng. A 61 (2004) 378.
[24] H. Sehitoglu, I. Karaman, R. Anderson, X. Zhang, K. Gall, H.J. Maier, Y.I. Chumlyakov, Acta Mater. 48 (2000) 3311.
[25] H.E. Karaca, I. Karaman, Y.I. Chumlyakov, D.C. Lagoudas, X. Zhang, Scr. Mater. 51 (2004) 261.
[26] J. Dadda, H.J. Maier, D. Niklasch, I. Karaman, H.E. Karaca, Y.I. Chumlyakov, Metall. Mater. Trans. A 39A (2008) 2026.
[27] S. Kajiwara, Mater. Sci. Eng. A 273 (1999) 67.
[28] W.F. Hosford, Mechanical Behavior of Materials, Cambridge University Press, Cambridge, 2005.
[29] G.I. Taylor, C.F. Elam, Proc. R. Soc. A 112 (1926) 337.
[30] T. Yalcinkaya, W.A.M. Brekelmans, M.G.D. Geers, Model. Simul. Mater. Sci. Eng. 16 (2008) 085007.